Production of neutron-rich nuclei near $N = 126$ in multinucleon transfer reactions with potential pockets

Gen Zhang [1,*] and Feng-Shou Zhang [2]

[1]*Guangxi Key Laboratory for Relativistic Astrophysics, School of Physical Science and Technology, Guangxi University, Nanning 530004, China*

[2]*The Key Laboratory of Beam Technology of Ministry of Education, College of Nuclear Science and Technology, Beijing Normal University, Beijing 100875, China*

(Received 31 October 2024; accepted 19 December 2024; published 8 January 2025)

The quasifission rate is improved by the harmonic oscillator approximation for the interaction potential at the barrier and pocket. Within the framework of the DNS model, the calculated production cross sections are in good agreement with the experimental data in ^{64}Ni + ^{208}Pb reaction. The dependence of the cross sections on the isospin of the reaction partner is studied. The cross sections of neutron-rich isotopes in the reaction with the reaction partner having the highest N/Z ratio are the largest, because of the lowest difference of potential energy surface and driving potential. As the scattering angle is smaller than the smaller rainbow angle, the differential cross section of the fragment decreases sharply, because of the much smaller partial cross section at a lower angular momentum. The angular distribution shifts to a larger angle at a higher incident energy. The angular distribution of the unknown isotopes near $N = 126$ in ^{70}Ni + ^{202}Pt reaction is located at 75°–150° and peaks at about 80°.

DOI: 10.1103/PhysRevC.111.014603

I. INTRODUCTION

The production of unknown isotopes is one of the frontiers in nuclear physics, which is important for the investigation of nuclear structure and properties, such as the nuclear halo, shell evolution, exotic decay modes, single-particle levels, and more [1,2]. According to the theoretical predictions, there are still more than 4000 unknown radioactive nuclei, primarily in the neutron-rich and superheavy regions [3,4]. While the neutron-drip line has been reached in the light-mass region, a lot of neutron-rich isotopes with medium and heavy masses remain unexplored. The neutron-rich nuclei near $N = 126$ are particularly significant to investigate the r-process in nuclear astrophysics, because $N = 126$ is the last "waiting point" in r-process path [5–7]. The study on the properties of these nuclei, such as their abilities of neutron capture and β decay rates, is helpful to solve the puzzle of the origin of the heavy elements heavier than iron.

Nowadays, the neutron-rich nuclei near $N = 126$ are mainly produced by projectile fragmentation reactions [8,9]. However, the production cross sections by that method are rather low. Based on the stable projectile-target combination, only neutron-deficient nuclei have been synthesized using fusion reactions. During the past decade, the multinucleon transfer reaction (MNT) has been proposed as a promising method to produce neutron-rich and superheavy nuclei [10,11]. MNT is a dissipative process in which many nucleons flow between the projectile and target, allowing a wide range of isotopes to be produced far from the entrance channel. A series of experiments on MNT reactions has been conducted since 1970s [12–20]. Until 1995, 76 unknown isotopes of elements from carbon to thorium had been generated by MNT reactions, and all of them fell in the neutron-rich region [21]. For example, 17 new neutron-rich nuclei with $Z = 12$–17 were detected in the collision of ^{40}Ar + ^{232}Th at Dubna [12]. After twenty years, the experiment on the transfer reaction ^{48}Ca + ^{248}Cm was conducted at GSI in 2015, and five unknown isotopes with $Z = 92$–97 were identified [22]. Last year, a new isotope ^{241}U near the deformed shell closure at $N = 152$ was observed in the MNT reaction of ^{238}U + ^{198}Pt at RIKEN [23]. To produce the neutron-rich isotopes near $N = 126$, the MNT reactions of ^{136}Xe + ^{208}Pb [24,25], ^{136}Xe + ^{198}Pt [26,27], and ^{204}Hg + ^{198}Pt [28] were performed at Dubna, Argonne, and GANIL. Although no unknown isotopes were observed, the cross sections of $N = 126$ isotones were much larger than those achieved through projectile fragmentation reactions. Recently, there have been several facilities under construction, such as the $N = 126$ factory at Argonne [29] and the High-Energy Fragment Separator (HFRS) at HIAF [30], for the study of the production and properties of neutron-rich nuclei near $N = 126$.

During the past decades, various models have been developed to describe the MNT reactions. The macroscopic models, such as the GRAZING model [31,32], Langevin equations [33–35], complex Wentzel-Kramers-Brillouin (CWKB) model [36], and dinuclear system (DNS) model [37,38], can describe the dissipation of total kinetic energy, angular momentum, and the diffusion of charge, mass and N/Z ratio. The microscopic models, including time-dependent Hartree-Fock (TDHF) model [39,40], the improved quantum molecular dynamics (ImQMD) model [41,42], and time-dependent

*Contact author: zhanggen@gxu.edu.cn

covariant density functional theory (TD-CDFT) [43], based on the mean-field, have successfully described the dynamical evolution of nucleons. DNS model is a semiclassical macroscopic model, in which the nucleon diffusion is described by the master equation. It has been widely applied to investigate the mechanism in fusion [44] and MNT [45] reactions and to predict the production cross sections of unknown isotopes.

In this paper, we improve the calculation of quasifission rate in master equation by harmonic oscillator approximation. The isospin effect of the projectile and target is studied, and the angular distribution of the unknown isotopes near $N = 126$ is predicted. This article is organized as follows. In Sec. II, the framework of DNS model is introduced. Subsequently, the calculated results by the DNS model and the discussion are presented in Sec. III. Finally, a summary is provided in Sec. IV.

II. THE MODEL

In the DNS model, the time evolution of the probability of the fragment with proton number Z_1 and neutron number N_1 is described by the master equation, expressed as follows [46]:

$$\frac{dP(Z_1,N_1,t)}{dt} = \sum_{Z_1'} W_{Z_1,N_1;Z_1',N_1}(t)\left[d_{Z_1,N_1}P(Z_1',N_1,t) - d_{Z_1',N_1}P(Z_1,N_1,t)\right] + \sum_{N_1'} W_{Z_1,N_1;Z_1,N_1'}(t)\left[d_{Z_1,N_1}P(Z_1,N_1',t) - d_{Z_1,N_1'}P(Z_1,N_1,t)\right] - \Lambda_{\rm qf}(t)P(Z_1,N_1,t). \quad (1)$$

Here, $W_{Z_1,N_1;Z_1',N_1}$ denotes the mean transition probability from the channel (Z_1,N_1) to (Z_1',N_1) channel. d_{Z_1,N_1} represents the microscopic dimension corresponding to the macroscopic state (Z_1,N_1). The sum is taken over all proton and neutron numbers that one fragment can have, but only one proton or neutron transfer is considered in every time step to simplify the case. $\Lambda_{\rm qf}$ is the quasifission rate, which is calculated by one-dimensional Kramers equation as follows [47,48]:

$$\Lambda_{\rm qf} = \frac{\omega_{\rm b}}{2\pi\omega_{\rm t}}\left[\sqrt{\left(\frac{\Gamma}{2\hbar}\right)^2+\omega_t^2} - \frac{\Gamma}{2\hbar}\right]\exp\left[-\frac{B_{\rm qf}(Z_1,N_1)}{\Theta(t)}\right], \quad (2)$$

where Γ is the double average width of the single-particle state, taken as $\Gamma = 2.8$ MeV. $B_{\rm qf}$ is the quasifission barrier of the DNS. Θ denotes the local temperature, which is calculated by the Fermi-gas expression $\Theta = \sqrt{\epsilon^*/a}$, where ϵ^* is the local excitation energy and a is the level-density parameter taken as $a = A/12$ MeV^{-1}. The two frequencies $\omega_{\rm b}$ and $\omega_{\rm t}$ denote the frequency of the harmonic oscillator approximating the potential at the bottom of the potential pocket and the top of the potential barrier, respectively, which are usually taken as constants, namely, $\hbar\omega_{\rm b} = 3$ MeV and $\hbar\omega_{\rm t} = 2$ MeV. However, the frequencies are dependent on the DNS because of the different interaction potential. In the Fig. 1, the interaction potential in the reaction ^{48}Ca + ^{208}Pb (a) and ^{58}Ni + ^{208}Pb (b) are shown. It can be found that the potential by harmonic oscillator approximation (HOA) is closer to the interaction potential at the potential pocket and potential barrier. Therefore, we calculated the frequencies according to HOA in this work, expressed as follows:

$$\omega_{\rm b} = \sqrt{\frac{1}{\mu}\frac{\partial^2}{\partial r^2}V(r)}\bigg|_{r=r_{\rm b}}, \quad (3)$$

and

$$\omega_{\rm t} = \sqrt{-\frac{1}{\mu}\frac{\partial^2}{\partial r^2}V(r)}\bigg|_{r=r_{\rm t}}. \quad (4)$$

The nucleon transfer process is determined by the single-particle potential. The proton transition probability is given by the following equation [46]:

$$W_{Z_1,N_1;Z_1',N_1} = \frac{\tau_{\rm mem}(Z_1,N_1,\epsilon_1;Z_1',N_1,\epsilon_1')}{d_{Z_1,N_1}d_{Z_1',N_1}\hbar^2} \times \sum_{i,i'}|\langle Z_1',N_1,\epsilon_1',i'|V(t)|Z_1,N_1,\epsilon_1,i\rangle|^2. \quad (5)$$

Here, ϵ is the local excitation energy of DNS, $\tau_{\rm mem}$ represents the memory time, and $V(t)$ denotes the single-particle potential resulting from the DNS mean-field. d_{Z_1,N_1} indicates the microscopic dimension of the fragment (Z_1,N_1), which is determined by the number of valence nucleons m_k in the valence space $\Delta\epsilon_k$ opened by the local excitation energy ϵ_k, expressed as [49]

$$d_{Z_1,N_1} = C_{n_1}^{m_1}\times C_{n_2}^{m_2}, \quad (6)$$

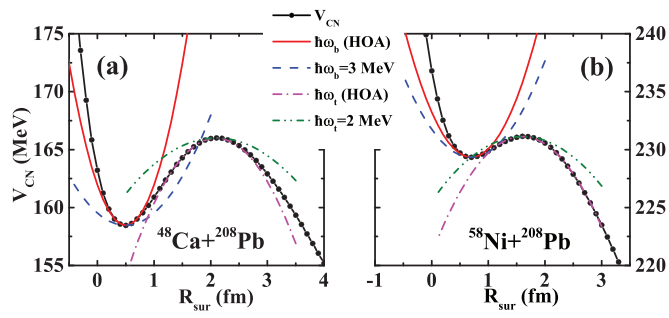

FIG. 1. The interaction potential in the reactions ^{48}Ca + ^{208}Pb (a) and ^{58}Ni + ^{208}Pb (b), represented by the solid circles. The dashed and dash-dot-dotted lines denote the potential at pocket with $\hbar\omega_{\rm b} = 3$ MeV and the potential at barrier with $\hbar\omega_{\rm t} = 2$ MeV, respectively. The solid and dash-dotted lines represent the results by harmonic oscillator approximation.

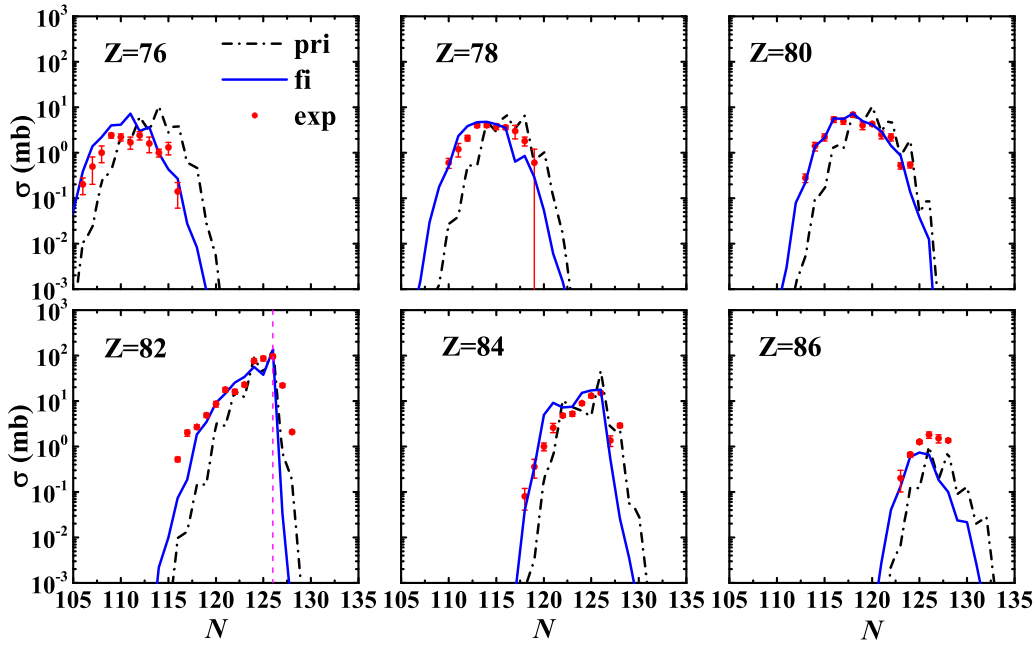

FIG. 2. The production cross sections of the isotopes with $Z = 76$–86 in the reaction ^{64}Ni + ^{208}Pb at $E_{\rm lab} = 350$ MeV. The dash-dotted and solid lines denote the primary and final cross sections, respectively. The experimental data is represented by solid circles, taken from Ref. [57].

where n_1 is the number of valence states in the valence space of projectile-like fragment (PLF), and n_2 corresponds to the case of target-like fragment (TLF). It is calculated as $n_k = g_k \Delta\varepsilon_k$ ($k = 1, 2$), in which g_k is the mean single-particle level density, typically $g_k = A_k/12$. The valence space $\Delta\varepsilon_k$ is calculated by $\Delta\varepsilon_k = 2\sqrt{\varepsilon_k g_k}$, where ε_k is the excitation energy of the fragment k. The number of valence nucleons is half of the number of valence states, shown as $m_k = n_k/2$. The expression of neutron transition probability is similar to that for proton transition.

The local excitation energy of DNS can be deduced as follows:

$$\epsilon = E_{\rm c.m.} + Q_{\rm gg} - V_{\rm CN} - \frac{\langle J(t)\rangle^2}{2\zeta_{\rm rel}} - \frac{(J_i - \langle J(t)\rangle)^2}{2\zeta_{\rm int}} - \langle E_{\rm rad}(J,t)\rangle. \quad (7)$$

Here, $Q_{\rm gg} = \Delta_{\rm P} + \Delta_{\rm T} - \Delta_{\rm PLF} - \Delta_{\rm TLF}$, where $\Delta_{\rm P}$, $\Delta_{\rm T}$, $\Delta_{\rm PLF}$, and $\Delta_{\rm TLF}$ represent the mass excesses of projectile, target, PLF, and TLF, respectively. The mass excess is taken the experimental data, but that of the unknown isotope is calculated by Weizsäcker-Skyrme formula [50]. $V_{\rm CN}$ is sum of Coulomb potential and nuclear potential between the PLF and TLF at the potential pocket. The Coulomb potential is calculated by the deformation-dependent Wong formula [51], and the double-folding potential is applied for the nuclear potential [52]. $J_{\rm i}$ is the total angular momentum and $J(t)$ is the relative angular momenta at time t. $\zeta_{\rm rel}$ and $\zeta_{\rm int}$ indicate the relative and intrinsic moment of inertia of DNS, respectively. $E_{\rm rad}$ represents the radial kinetic energy.

The relative kinetic energy is dissipated into intrinsic excitation energy of DNS, and its time evolution can be derived from the Fokker-Planck equation,

$$\langle E_{\rm rad}(J,t)\rangle = E_{\rm rad}(J,0)\exp(-t/\tau_R), \quad (8)$$

where $E_{\rm rad}(J,0)$ is the radial kinetic energy at the initial time, and τ_R is its relaxation time, taken as $\tau_R = 2 \times 10^{-22}$ s.

The relative angular momentum is dissipated into the intrinsic angular momentum, relaxed from the incident angular momentum to the value at the sticking limit,

$$\langle J(t)\rangle = J_{\rm st} + (J_{\rm i} - J_{\rm st})\exp(-t/\tau_J), \quad (9)$$

Here, $J_{\rm st}$ indicates the angular momentum at the sticking limit, expressed as $J_{\rm st} = \zeta_{\rm rel}/\zeta_{\rm tot} J_{\rm i}$, and $J_{\rm i}$ denotes the angular momentum of the entrance channel. τ_J is the relaxation time of the angular momentum taken as 12×10^{-22} s, which is larger than τ_R, because the relaxation of angular momentum is slower than that of kinetic energy.

The two-dimensional isospin-dependent potential energy surface (PES) is vital to drive the nucleon diffusion, which is defined as the following [53]:

$$U(Z_1,N_1,Z_2,N_2,r_{\rm b}) = \Delta(Z_1,N_1) + \Delta(Z_2,N_2) + V_{\rm CN}(Z_1,N_1,Z_2,N_2,r_{\rm b}). \quad (10)$$

Here, the interaction potential $V_{\rm CN}$ consists of the Coulomb potential and nuclear potential, calculated by the deformation-dependent Wong formula [51] and double-folding potential with sudden approximation [52], respectively. $r_{\rm b}$ is the position of potential pocket that is considered as the distance between two fragments where nucleon transfer occurs.

Within the framework of DNS model, the primary cross section of the fragment with proton number Z and neutron

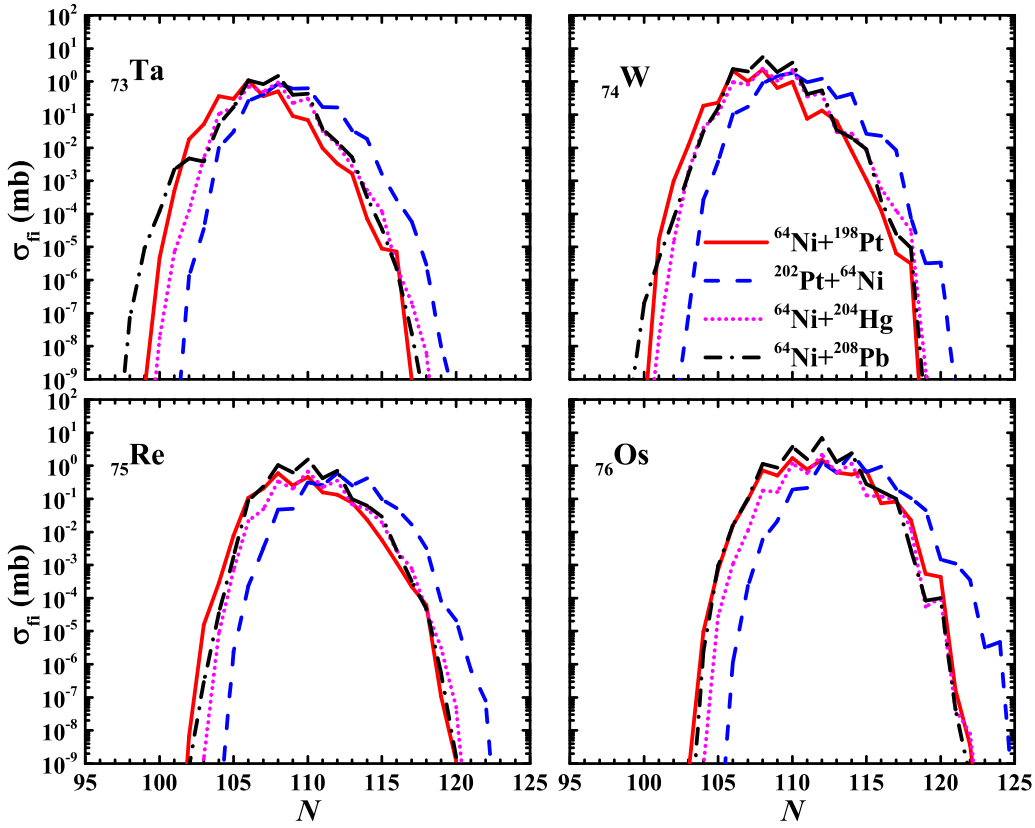

FIG. 3. The final production cross sections of the fragments with $Z = 73$–76 in the reactions ^{64}Ni + ^{198}Pt, ^{202}Pt + ^{64}Ni, ^{64}Ni + ^{204}Hg, and ^{64}Ni + ^{208}Pb, denoted by the solid, dashed, dotted, and dash-dotted lines, respectively.

number N can be expressed as

$$\sigma_{\rm pri}(Z,N) = \frac{\pi\hbar^2}{2\mu E_{\rm c.m.}} \sum_{J=0}^{J_{\rm max}} (2J+1)[P(Z,N,\tau_{\rm int}) + Y_{\rm qf}(Z,N,\tau_{\rm int})]. \quad (11)$$

Here, μ is the reduced mass in the entrance channel, and the maximum angular momentum $J_{\rm max}$ is taken as the value at grazing collision. $P(Z,N,\tau_{\rm int})$ is the distribution probability of fragment (Z,N) at the interaction time $\tau_{\rm int}$, which is calculated by the classical deflection function method [54]. Beside the fragment from the diffusion process, the contribution of the quasifission through the interaction time should be included in the production cross section. The quasifission yield is defined as [53]

$$Y_{\rm qf}(Z,N) = \int_0^{\tau_{\rm int}} \Lambda_{\rm qf} P(Z,N,t)dt. \quad (12)$$

The excitation energy of the primary fragment is supposed to be proportional to its mass, namely, $\epsilon_k = \epsilon A_k/A_{\rm CN}$, in which $A_{\rm CN}$ is the mass number of the compound nucleus. To predict the production cross sections of the final fragments, the GEMINI + + code is applied to calculate the probability of neutron and charged-particle evaporation based on a Monte Carlo method [55,56].

III. RESULTS AND DISCUSSION

To verify the reliability of the DNS model for the description of MNT reaction, the production cross sections of the isotopes with $Z = 76$–86 in the reaction ^{64}Ni + ^{208}Pb at $E_{\rm lab} =$ 350 MeV are calculated, as shown in Fig. 2. One can see that the calculated final cross sections reproduce the experimental data very well. The fission barrier of these nuclei is very high, so the main deexcitation mode is neutron evaporation. The cross sections of the trans-target isotopes decrease more sharply with increase in the number of transferred protons, compared with the below-target isotopes. That is caused by the proton shell closure of $Z = 82$ of the target, making it hard to pickup protons from the projectile. Finding the optimal projectile-target combination to produce the unknown isotope is extremely important for the nuclear experiments. The final production cross sections of the fragments with $Z = 73$–76 in the reactions with ^{64}Ni are shown in Fig. 3. The N/Z ratios of the heavier reaction partners, ^{198,202}Pt, ^{204}Hg, and ^{208}Pb, are 1.538, 1.589, 1.55, and 1.536, respectively. It can be noticed that the cross sections of neutron-rich isotopes in the reaction with ^{202}Pt are the highest, because its N/Z ratio is the largest. According to the mechanism of equilibrium of N/Z ratio in MNT reactions, the reaction partner with higher N/Z ratio is advantageous for producing neutron-rich nuclei. Actually, the nucleon diffusion process is driven by the PES. The ΔU is defined as $\Delta U = U(Z_{\rm PLF}, N_{\rm PLF}, Z_{\rm TLF}, N_{\rm TLF}, r_b) - U(Z_{\rm P}, N_{\rm P}, Z_{\rm T}, N_{\rm T}, r_b)$, which is the difference in the potential

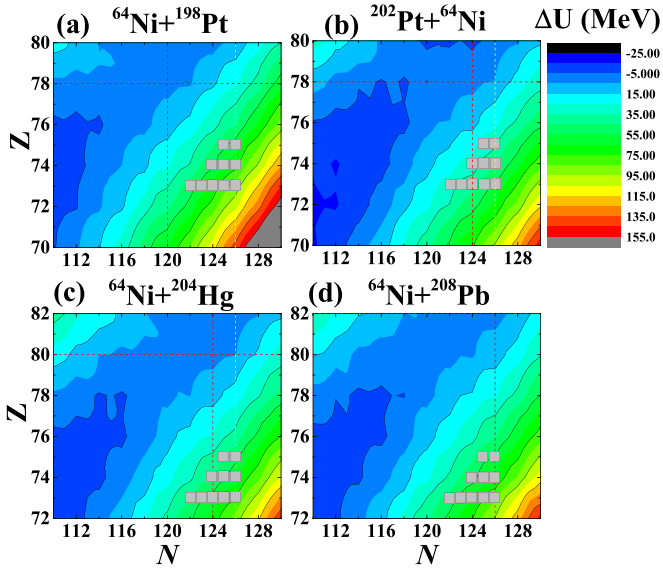

FIG. 4. The ΔU value in the reactions $^{64}\mathrm{Ni}+^{198}\mathrm{Pt}$ (a), $^{202}\mathrm{Pt}+^{64}\mathrm{Ni}$ (b), $^{64}\mathrm{Ni}+^{204}\mathrm{Hg}$ (c), and $^{64}\mathrm{Ni}+^{208}\mathrm{Pb}$ (d). The grey squares mark the unknown isotopes near $N = 126$.

energy surface between the primary fragment and entrance channel. In general, the fragments with smaller ΔU have larger cross sections. The results of ΔU in the four reactions mentioned above are shown in Fig. 4. The grey squares mark the unknown isotopes near $N = 126$. It is evident that the ΔU value of the unknown nuclei in $^{202}\mathrm{Pt}+^{64}\mathrm{Ni}$ is the lowest, resulting in the highest production cross section. The ΔU of the unknown isotopes in the other reactions are pretty close, so the difference of the cross sections in those nuclei is not significant. To investigate the dependence of the production cross sections on the lighter reaction partner, we calculated the cross sections of the fragments with $Z = 73$–76 in the reactions $^{202}\mathrm{Pt}+^{48}\mathrm{Ca}$, $^{202}\mathrm{Pt}+^{64}\mathrm{Ni}$, and $^{70}\mathrm{Ni}+^{202}\mathrm{Pt}$, displayed in Fig. 5. The N/Z ratios of ^{48}Ca and ^{64,70}Ni are 1.4, 1.285, and 1.5, respectively. One can find that the cross sections of neutron-rich nuclei in the reaction with ^{70}Ni are the largest, which is also owing to the highest N/Z ratio of ^{70}Ni, making the heavier reaction partner more likely to pickup neutrons while stripping protons. From the driving potential, one can roughly analyze the trend of nucleon transfer. In Fig. 6, the driving potential in the three reactions mentioned above is shown. The dashed line marks the mass number of ^{202}Pt. It is obvious that as more nucleons are stripped from ^{202}Pt, the driving potential in the reaction $^{70}\mathrm{Ni}+^{202}\mathrm{Pt}$ becomes lower.

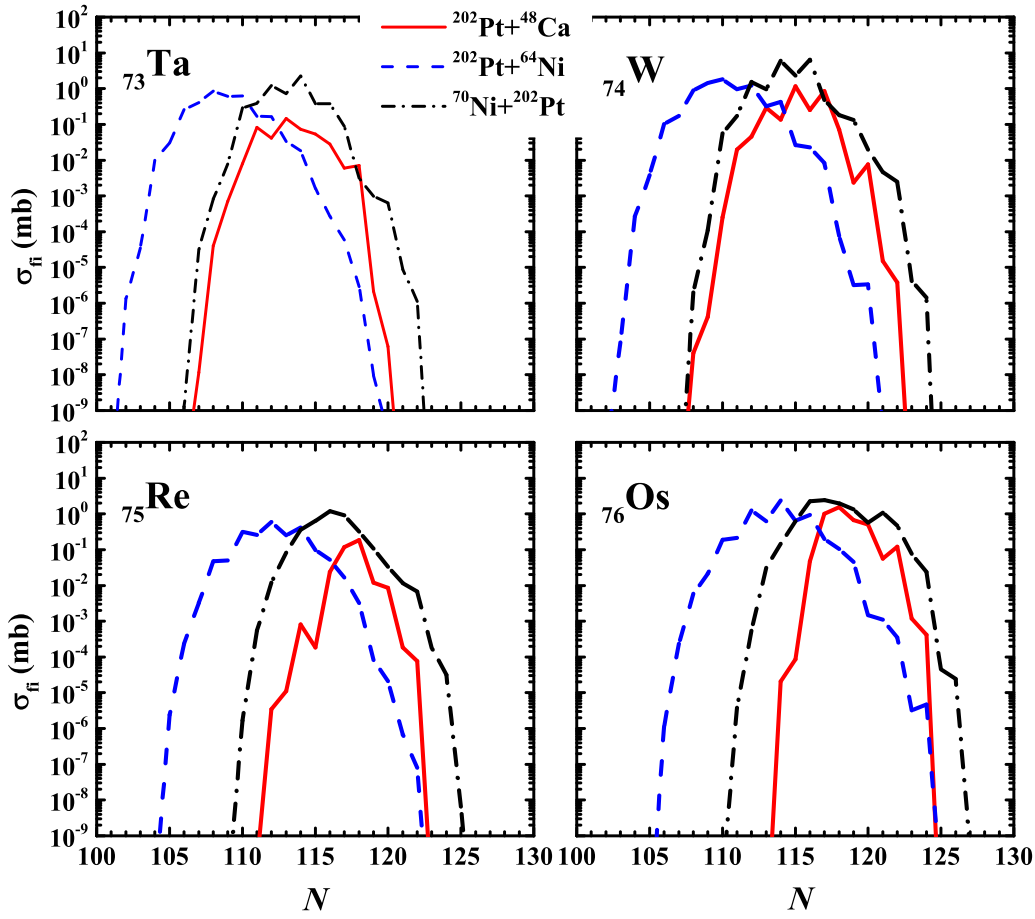

FIG. 5. The final production cross sections of the fragments with $Z = 73$–76 in the reactions $^{202}\mathrm{Pt}+^{48}\mathrm{Ca}$, $^{202}\mathrm{Pt}+^{64}\mathrm{Ni}$, and $^{70}\mathrm{Ni}+^{202}\mathrm{Pt}$, denoted by the solid, dashed, and dash-dotted lines, respectively.

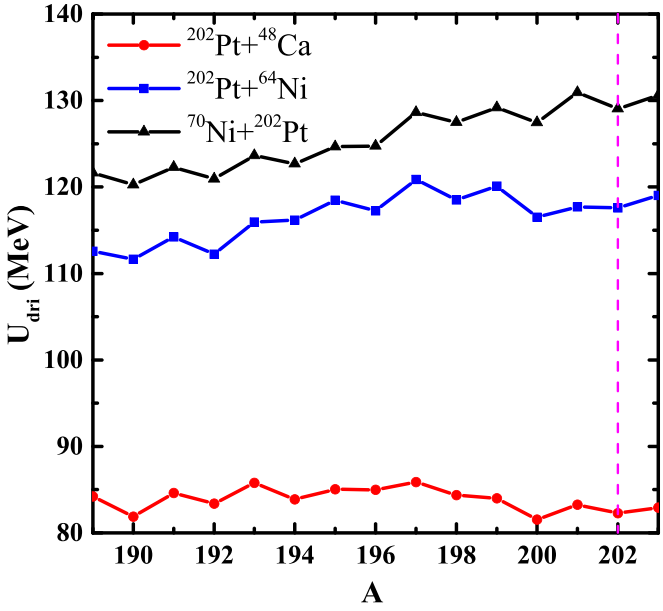

FIG. 6. The driving potential in the reactions $^{202}\mathrm{Pt}+^{48}\mathrm{Ca}$, $^{202}\mathrm{Pt}+^{64}\mathrm{Ni}$, and $^{70}\mathrm{Ni}+^{202}\mathrm{Pt}$, represented by the solid circles, squares, and triangles, respectively. The dash line marks the mass number of ^{202}Pt.

However, the driving potential in the other two reactions does not change significantly, especially in $^{202}\mathrm{Pt}+^{48}\mathrm{Ca}$ reaction. Therefore, the nucleons are easier to be transferred to ^{70}Ni, which is more favorable for producing neutron-rich isotopes with smaller proton number. The angular distribution of the fragment is very significant for the experiment to place the detector in the appropriate position. Within the framework of the DNS model, the angular distribution can be investigated by the defection function method [54]. In Fig. 7(a), the angular distribution of the primary fragment ^{190}W in $^{70}\mathrm{Ni}+^{202}\mathrm{Pt}$ reaction at $E_{\mathrm{c.m.}} = 1.2\ V_{\mathrm{C}}$ is shown. One can see that the angular distribution mainly concentrates on the range of 90°–140°. As the scattering angle is smaller than 90°, the differential cross section decreases sharply. From the deflection function of the TLF displayed in Fig. 7(c), it is evident that there are two rainbow angles. The larger one is about 140°, which is the largest scattering angle. The dashed line marks the position of the smaller rainbow angle. Therefore, the angular distribution of the fragment is mainly between two rainbow angles. This phenomenon can be explained from the primary partial cross sections shown in Fig. 7(b), denoted by the solid line. The dashed line represents the smaller rainbow angle. One can find that as the scattering angle is smaller than the smaller rainbow angle, the quantum number of

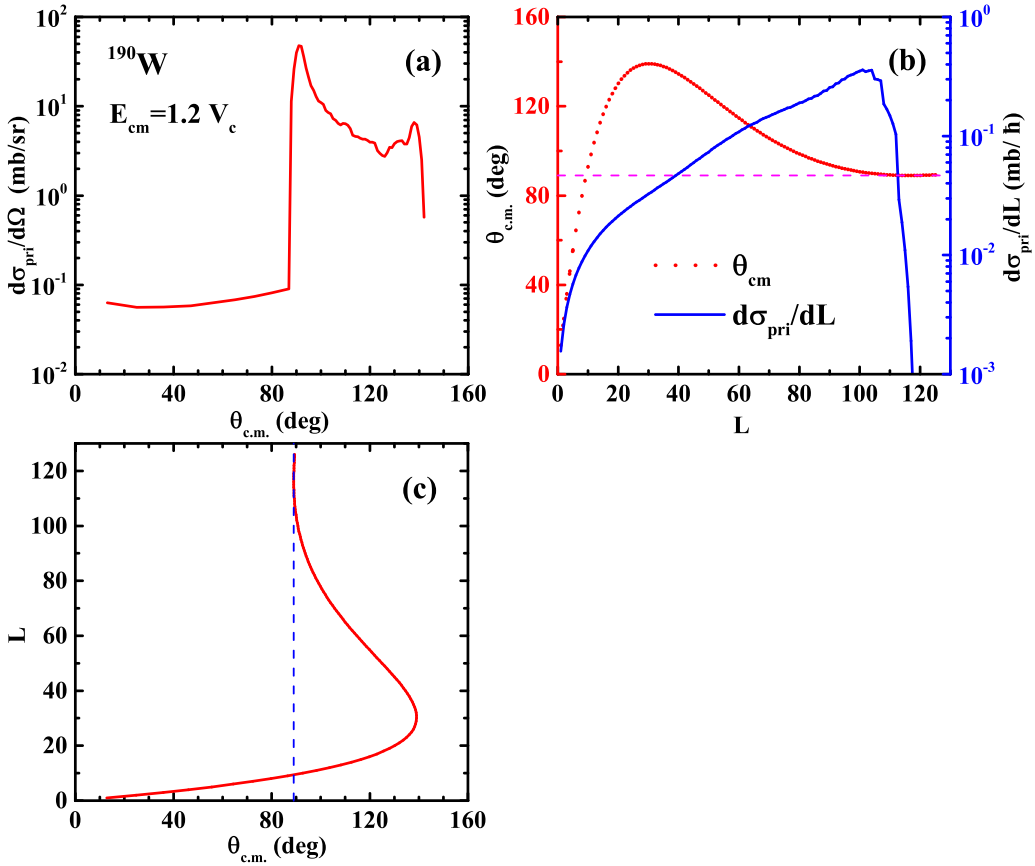

FIG. 7. (a) The primary angular distribution of the fragment ^{190}W in center-of-mass system in $^{70}\mathrm{Ni}+^{202}\mathrm{Pt}$ reaction at $E_{\mathrm{c.m.}} = 1.2\ V_{\mathrm{C}}$. (b) The deflection function of the TLF denoted by the dotted line. The solid line represents the primary partial cross sections of ^{190}W. (c) The deflection function of the TLF.

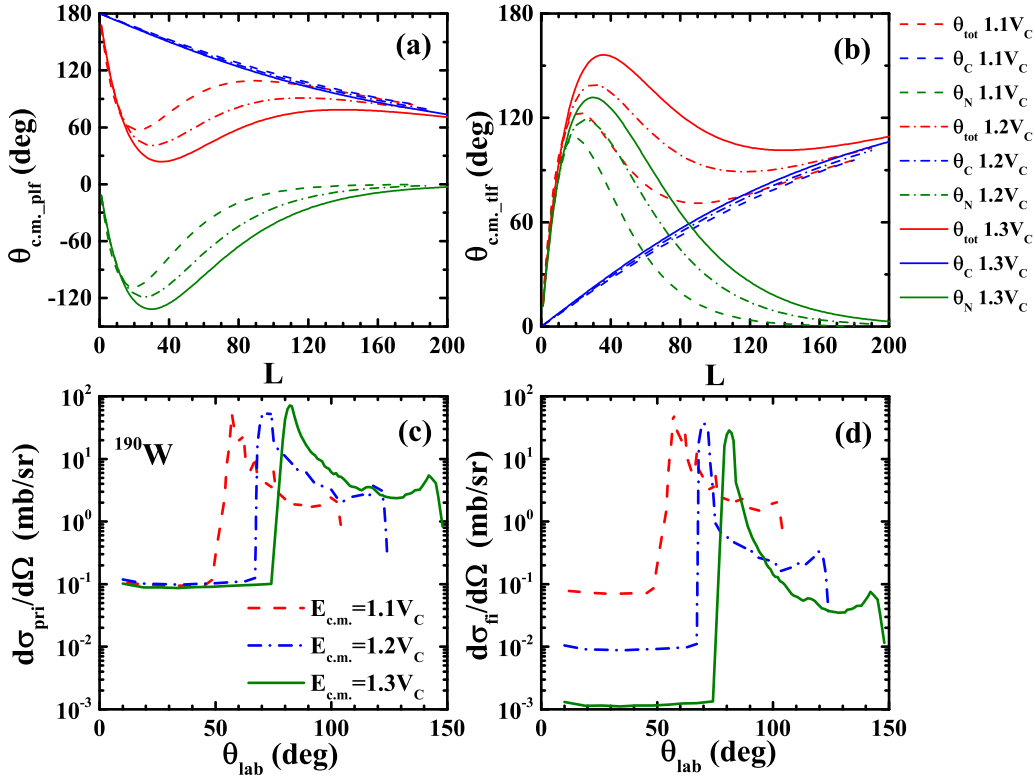

FIG. 8. The deflection function of the PLF (a) and TLF (b) in the reaction ^{70}Ni + ^{202}Pt. The red, blue, and olive lines represent the total, Coulomb, and nuclear scattering angle, respectively. The angular distribution of the primary fragment ^{190}W (c) and final fragment ^{190}W (d). The dashed, dash-dotted, and solid lines correspond to the case at 1.1 V_C, 1.2 V_C, and 1.3 V_C, respectively.

angular momentum L is smaller than 10, leading to a rather small partial cross section. In general, the production cross sections of the neutron-rich isotopes is not sensitive to the incident energy, because the primary neutron-rich fragment can evaporate more nucleons at a higher incident energy. However, the angular distribution of the fragment is dependent on the incident energy. The deflection function of the PLF and TLF is shown in Figs. 8(a) and 8(b), respectively. It can be found that the Coulomb scattering angle is not sensitive to the incident energy, especially at a low angular momentum. The nuclear scattering angle of the PLF becomes more negative as the incident energy increases, meaning that the nuclear potential is more attractive at a higher energy, which results in a decline of the total scattering angle. For the TLF, the dependence of the nuclear and total scattering angles on the incident energy is opposite, because the scattering angle of TLF is the complementary angle of that of PLF. In this paper, we are concerned with the angular distribution of TLF. The angular distribution of the primary fragment ^{190}W and final fragment ^{190}W, is shown in Figs. 8(c) and 8(d), respectively. One can notice that the angular distribution shifts to a larger angle at a higher incident energy, because the scattering angle of TLF is larger. Comparing the primary and final differential cross sections, the final results are lower than the primary. In addition, the decline of the differential cross sections at 1.3 V_C is the most significant, because the excitation energy of the primary fragment is the highest, leading to the smallest survival probability. The angular distribution of the unknown isotopes near $N = 126$ in ^{70}Ni + ^{202}Pt reaction at $E_{c.m.} = 1.3\ V_C$ is displayed in Fig. 9. The calculated differential cross sections of Ta, W, and Re isotopes are shown in Figs. 9(a), 9(b), and 9(c), respectively. One can find that the angular distribution of all the fragments is in the range 75°–150° and peaks at about 80°. For the isotopes of the same element, the differential cross sections of more neutron-rich isotopes are smaller because of the smaller primary production cross sections.

However, one should notice that in the reaction ^{70}Ni + ^{202}Pt, both the projectile and target are radioactive. Based on the current experimental conditions, it is hard to perform that collision in the experiments. If the intensity of the ^{70}Ni beam is improved in the facilities for radioactive beams and the thickness of the target is increased in the future, the production of new isotopes near $N = 126$ is probable.

IV. SUMMARY

The quasifission rate is improved by the harmonic oscillator approximation for the interaction potential at the barrier and pocket. Within the framework of the DNS model, the calculated production cross sections are in good agreement with the experimental data in the ^{64}Ni + ^{208}Pb reaction. The dependence of the cross sections on the isospin of the reaction partner is studied. The cross sections of neutron-rich isotopes in the reaction with ^{202}Pt are the highest, because of the mechanism of equilibrium of N/Z ratio in MNT

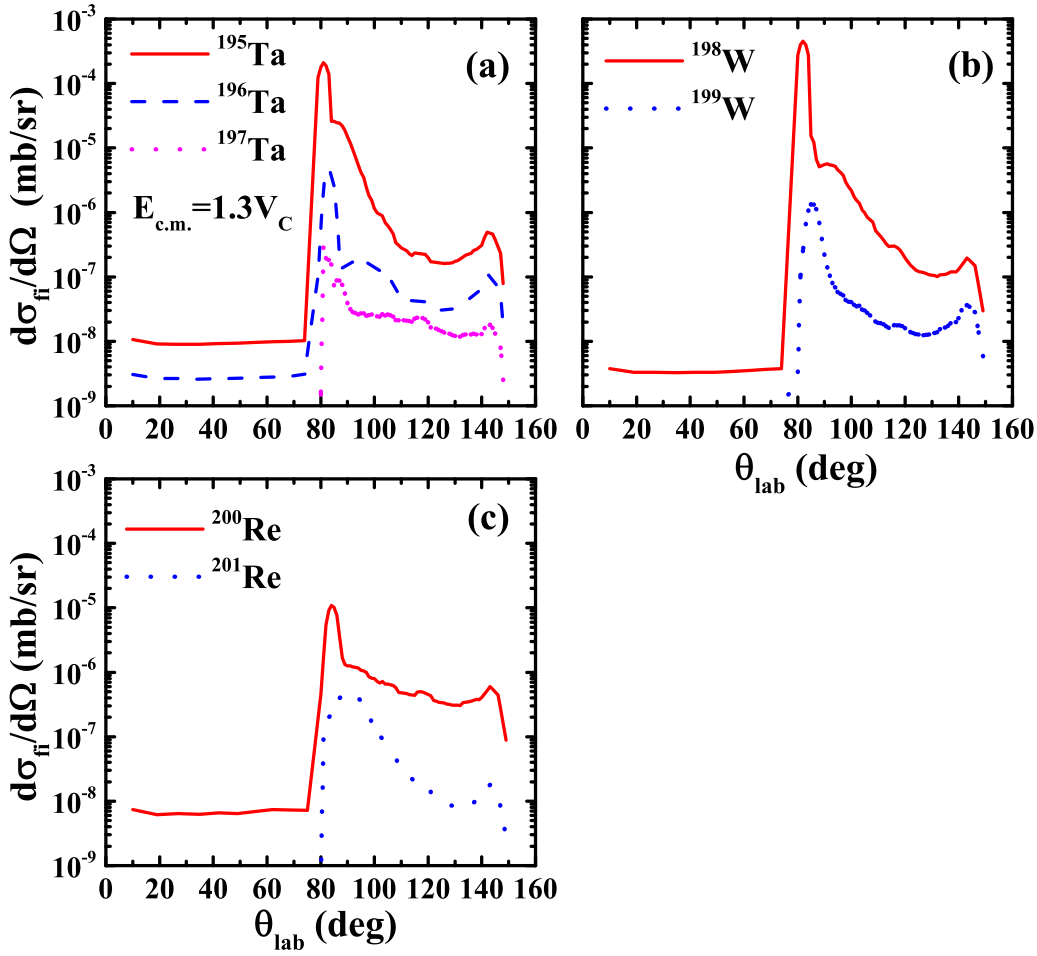

FIG. 9. The angular distribution of the unknown isotopes in ^{70}Ni + ^{202}Pt reaction at $E_{c.m.} = 1.3\ V_C$. (a) The angular distribution of the final fragment ^{195}Ta, ^{196}Ta, and ^{197}Ta, denoted by solid, dashed, and dotted lines, respectively. (b) The solid and dotted lines represent the results of ^{198}W and ^{199}W, respectively. (c) The angular distribution of ^{200}Re (solid line) and ^{201}Re (dotted line).

reactions. In addition, the ΔU value of the unknown nuclei in ^{202}Pt + ^{64}Ni is the lowest, resulting in the highest production cross section. Similarly, the cross sections of neutron-rich nuclei in the reaction with ^{70}Ni are the largest, because more nucleons are stripped from the heavier reaction partner, the driving potential in the reaction ^{70}Ni + ^{202}Pt becomes lower. Therefore, the nucleons are easier to be transferred to ^{70}Ni, which is more favorable to produce neutron-rich isotopes with a smaller proton number.

As the scattering angle is smaller than the smaller rainbow angle, the differential cross section decreases sharply because of a rather small partial cross section at $L < 10$. The angular distribution of the fragment is dependent on the incident energy. The Coulomb scattering angle is not sensitive to the incident energy, while the nuclear scattering angle of the PLF becomes more negative as the incident energy increases, which results in a decline in the total scattering angle. The angular distribution shifts to a larger angle at a higher incident energy. The angular distribution of the unknown isotopes near $N = 126$ in ^{70}Ni + ^{202}Pt reaction is located at 75°–150° and peaks at about 80°.

ACKNOWLEDGMENTS

This work was supported by the Guangxi Natural Science Foundation under Grant No. 2022GXNSFBA035549 and the National Natural Science Foundation of China under Grant No. 12405145.

[1] Yu. T. Oganessian and V. K. Utyonkov, Rep. Prog. Phys. **78**, 036301 (2015).
[2] F. Nowacki, A. Obertelli, and A. Poves, Prog. Part. Nucl. Phys. **120**, 103866 (2021).
[3] P. Möller, A. J. Sierk, T. Ichikawa, and H. Sagawa, At. Data Nucl. Data Tables **109-110**, 1 (2016).
[4] A. V. Afanasjev, S. E. Agbemava, D. Ray, and P. Ring, Phys. Lett. B **726**, 680 (2013).

[5] E. M. Burbidge, G. R. Burbidge, W. A. Fowler, and F. Hoyle, Rev. Mod. Phys. **29**, 547 (1957).
[6] Y.-Z. Qian, Prog. Part. Nucl. Phys. **50**, 153 (2003).
[7] M. Arnould, S. Goriely, and K. Takahashi, Phys. Rep. **450**, 97 (2007).
[8] H. Alvarez-Pol, J. Benlliure, E. Casarejos, L. Audouin, D. Cortina-Gil, T. Enqvist, B. Fernández-Domínguez, A. R. Junghans, B. Jurado, P. Napolitani, J. Pereira, F. Rejmund, K.-H. Schmidt, and O. Yordanov, Phys. Rev. C **82**, 041602(R) (2010).
[9] J. Kurcewicz, F. Farinon, H. Geissel, S. Pietri, C. Nociforo, A. Prochazka, H. Weick, J. S. Winfield, A. Estradé, P. R. P. Allegro, A. Bail, G. Bélier, J. Benlliure, G. Benzoni, M. Bunce, M. Bowry, R. Caballero-Folch, I. Dillmann, A. Evdokimov, J. Gerl, A. Gottardo *et al.*, Phys. Lett. B **717**, 371 (2012).
[10] V. I. Zagrebaev, Yu. T. Oganessian, M. G. Itkis, and W. Greiner, Phys. Rev. C **73**, 031602(R) (2006).
[11] V. I. Zagrebaev and W. Greiner, J. Phys. G **35**, 125103 (2008).
[12] A. G. Artukh, V. V. Avdeichikov, G. F. Gridnev, V. L. Mikheev, V. V. Volkov, and J. Wilczński, Nucl. Phys. A **176**, 284 (1971).
[13] A. G. Artukh, G. F. Gridnev, V. L. Mikheev, V. V. Volkov, and J. Wilczynski, Nucl. Phys. A **215**, 91 (1973).
[14] F. Hanappe, M. Lefort, C. Ngô, J. Péter, and B. Tamain, Phys. Rev. Lett. **32**, 738 (1974).
[15] P. Auger, T. H. Chiang, J. Galin, B. Gatty, D. Guerreau, E. Nolte, J. Pouthas, X. Tarrago, and J. Girard, Z. Phys. A **289**, 255 (1979).
[16] D. Guerrau, J. Galin, B. Gatty, X. Tarrago, J. Girard, R. Lucas, and C. Ngô, Z. Phys. A **295**, 105 (1980).
[17] H. Breuer, K. L. Wolf, B. G. Glagola, K. K. Kwiatkowski, A. C. Mignerey, V. E. Viola, W. W. Wilcke, W. U. Schröder, J. R. Huizenga, D. Hilscher, and J. Birkelund, Phys. Rev. C **22**, 2454 (1980).
[18] R. Kirchner, O. Klepper, W. Kurcewicz, E. Roeckl, E. F. Zganjar, E. Runte, W.-D. Schmidt-Ott, P. Tidemand-Petersson, N. Kaffrell, P. Peuser, and K. Rykaczewski, Nucl. Phys. A **378**, 549 (1982).
[19] E. Runte, W.-D. Schmidt-Ott, P. Tidemand-Petersson, R. Kirchner, O. Klepper, W. Kurcewicz, E. Roeckl, N. Kaffrell, P. Peuser, K. Rykaczewski, M. Bernas, P. Dessagne, and M. Langevin, Nucl. Phys. A **399**, 163 (1983).
[20] C. Wennemann, W.-D. Schmidt-Ott, T. Hild, K. Krumbholz, V. Kunze, F. Meissner, H. Keller, R. Kirchner, and E. Roeckl, Z. Phys. A **347**, 185 (1994).
[21] S. Heinz and H. M. Devaraja, Eur. Phys. J. A **58**, 114 (2022).
[22] H. M. Devaraja, S. Heinz, O. Beliuskina, V. Comas, S. Hofmann, C. Hornung, G. Münzenberg, K. Nishio, D. Ackermann, Y. K. Gambhir, M. Gupta, R. A. Henderson, F. P. Heßberger, J. Khuyagbaatar, B. Kindler, B. Lommel, K. J. Moody, J. Maurer, R. Mann, A. G. Popeko, D. A. Shaughnessy *et al.*, Phys. Lett. B **748**, 199 (2015).
[23] T. Niwase, Y. X. Watanabe, Y. Hirayama, M. Mukai, P. Schury, A. N. Andreyev, T. Hashimoto, S. Iimura, H. Ishiyama, Y. Ito, S. C. Jeong, D. Kaji, S. Kimura, H. Miyatake, K. Morimoto, J.-Y. Moon, M. Oyaizu, M. Rosenbusch, A. Taniguchi, and M. Wada, Phys. Rev. Lett. **130**, 132502 (2023).
[24] E. M. Kozulin, E. Vardaci, G. N. Knyazheva, A. A. Bogachev, S. N. Dmitriev, I. M. Itkis, M. G. Itkis, A. G. Knyazev, T. A. Loktev, K. V. Novikov, E. A. Razinkov, O. V. Rudakov, S. V. Smirnov, W. Trzaska, and V. I. Zagrebaev, Phys. Rev. C **86**, 044611 (2012).
[25] J. S. Barrett, W. Loveland, R. Yanez, S. Zhu, A. D. Ayangeakaa, M. P. Carpenter, J. P. Greene, R. V. F. Janssens, T. Lauritsen, E. A. McCutchan, A. A. Sonzogni, C. J. Chiara, J. L. Harker, and W. B. Walters, Phys. Rev. C **91**, 064615 (2015).
[26] Y. X. Watanabe, Y. H. Kim, S. C. Jeong, Y. Hirayama, N. Imai, H. Ishiyama, H. S. Jung, H. Miyatake, S. Choi, J. S. Song, E. Clement, G. de France, A. Navin, M. Rejmund, C. Schmitt, G. Pollarolo, L. Corradi, E. Fioretto, D. Montanari, M. Niikura *et al.*, Phys. Rev. Lett. **115**, 172503 (2015).
[27] V. V. Desai, W. Loveland, K. McCaleb, R. Yanez, G. Lane, S. S. Hota, M. W. Reed, H. Watanabe, S. Zhu, K. Auranen, A. D. Ayangeakaa, M. P. Carpenter, J. P. Greene, F. G. Kondev, D. Seweryniak, R. V. F. Janssens, and P. A. Copp, Phys. Rev. C **99**, 044604 (2019).
[28] T. Welsh, W. Loveland, R. Yanez, J. S. Barrett, E. A. McCutchan, A. A. Sonzogni, T. Johnson, S. Zhu, J. P. Greene, A. D. Ayangeakaa, M. P. Carpenter, T. Lauritsen, J. L. Harker, W. B. Walters, B. M. S. Amro, and P. Copp, Phys. Lett. B **771**, 119 (2017).
[29] G. Savard, M. Brodeur, J. A. Clark, R. A. Knaack, and A. A. Valverde, Nucl. Instrum. Methods Phys. Res. Sect. B **463**, 258 (2020).
[30] S.-B. Ma, L.-N. Sheng, X.-H. Zhang, S.-T. Wang, K.-L. Wang, C.-W. Ma, H.-J. Ong, Z.-Y. Sun, S.-W. Tang, Y.-H. Yu, X.-T. Du, and X.-B. Wei, Nucl. Sci. Tech. **35**, 97 (2024).
[31] A. Winther, Nucl. Phys. A **572**, 191 (1994).
[32] R. Yanez and W. Loveland, Phys. Rev. C **91**, 044608 (2015).
[33] V. Zagrebaev and W. Greiner, Phys. Rev. Lett. **101**, 122701 (2008).
[34] S. Amano, Y. Aritomo, and M. Ohta, Phys. Rev. C **106**, 024610 (2022).
[35] V. V. Saiko and A. V. Karpov, Phys. Rev. C **109**, 064607 (2024).
[36] S. Szilner, L. Corradi, G. Pollarolo, S. Beghini, B. R. Behera, E. Fioretto, A. Gadea, F. Haas, A. Latina, G. Montagnoli, F. Scarlassara, A. M. Stefanini, M. Trotta, A. M. Vinodkumar, and Y. Wu, Phys. Rev. C **71**, 044610 (2005).
[37] G. G. Adamian, N. V. Antonenko, and W. Scheid, Nucl. Phys. A **618**, 176 (1997).
[38] P. W. Wen, A. K. Nasirov, C. J. Lin, and H. M. Jia, J. Phys. G **47**, 075106 (2020).
[39] K. Sekizawa and K. Yabana, Phys. Rev. C **93**, 054616 (2016).
[40] Z. Wu and L. Guo, Phys. Rev. C **100**, 014612 (2019).
[41] C. Li, F. Zhang, J. Li, L. Zhu, J. Tian, N. Wang, and F.-S. Zhang, Phys. Rev. C **93**, 014618 (2016).
[42] H. Yao and N. Wang, Phys. Rev. C **95**, 014607 (2017).
[43] D. D. Zhang, D. Vretenar, T. Nikšić, P. W. Zhao, and J. Meng, Phys. Rev. C **109**, 024614 (2024).
[44] X. J. Bao, S. Q. Guo, H. F. Zhang, and J. Q. Li, Phys. Rev. C **97**, 024617 (2018).
[45] Z. Liao, Z. Gao, Y. Yang, L. Zhu, and J. Su, Phys. Rev. C **109**, 054612 (2024).
[46] W. Nörenberg, Z. Phys. A **274**, 241 (1975).
[47] H. A. Kramers, Physica **7**, 284 (1940).
[48] G. G. Adamian, N. V. Antonenko, and W. Scheid, Phys. Rev. C **68**, 034601 (2003).
[49] S. Ayik, B. Schürmann, and W. Nörenberg, Z. Phys. A **279**, 145 (1976).
[50] M. Liu, N. Wang, Y. Deng, and X. Wu, Phys. Rev. C **84**, 014333 (2011).

[51] C. Y. Wong, Phys. Rev. Lett. **31**, 766 (1973).
[52] G. G. Adamian, N. V. Antonenko, R. V. Jolos, S. P. Ivanova, and O. I. Melnikova, Int. J. Mod. Phys. E **5**, 191 (1996).
[53] G. G. Adamian, N. V. Antonenko, and A. S. Zubov, Phys. Rev. C **71**, 034603 (2005).
[54] G. Wolschin and W. Nörenberg, Z. Phys. A **284**, 209 (1978).
[55] D. Mancusi, R. J. Charity, and J. Cugnon, Phys. Rev. C **82**, 044610 (2010).
[56] R. J. Charity, Phys. Rev. C **82**, 014610 (2010).
[57] W. Królas, R. Broda, B. Fornal, T. Pawłat, H. Grawe, K. H. Maier, M. Schramm, and R. Schubart, Nucl. Phys. A **724**, 289 (2003).